Hyperfine Interactions (2019) 240: 100
https://doi.org/10.1007/s10751-019-1640-5

Modified embedded-atom method potential for cadmium

M. O. Zacate[1]

Abstract
The second nearest-neighbor modified embedded atom method (2NN MEAM) is a semi-empirical simulation technique designed to calculate materials properties of metallic and covalent solids. It is a strong candidate for calculation of site occupation, defect association, and diffusion mechanisms in intermetallic compounds, which would provide a tool for interpreting experimental results and for predicting new, interesting measurements to perform. Potentials for 39 elements can be found in the literature, but cadmium, an important element for perturbed angular correlation spectroscopy (PAC), is absent. The purpose of this work was to develop a 2NN-MEAM potential for cadmium. Empirical parameters were determined through optimization of the potential's ability to reproduce known physical properties of pure cadmium including cohesive energy, lattice parameters, elastic constants, structural enthalpy differences, surface enthalpy, vacancy formation energy, thermal expansion, and specific heat. Prospects for using this new potential with 2NN MEAM potentials for other elements to help interpret previous PAC studies of cadmium diffusion in intermetallic compounds will be discussed.

Keywords Computer simulation · Semi-empirical model · Energy minimization · Molecular dynamics

1 Introduction

Computer simulations based on empirical potentials are well-established methods for calculating elastic, defect, surface, and thermal properties of materials. They are not well-suited for calculating magnetic fields and electric field gradients, so they are not used broadly in

---

This article is part of the Topical Collection on *Proceedings of the International Conference on Hyperfine Interactions and their Applications (HYPERFINE 2019), Goa, India, 10-15 February 2019*
Edited by S. N. Mishra, P. L. Paulose and R. Palit

✉ M. O. Zacate
zacatem1@nku.edu

[1] Department of Physics, Geology, and Engineering Technology, Northern Kentucky University, Highland Heights, KY 41099, USA

investigations of hyperfine interactions. Still, such simulations can be useful to researchers in this field, because empirical simulations can be used to predict which combinations of hyperfine radiotracers and materials compositions show promise for producing interesting experimental results. For example, empirical simulations can predict site occupation, i.e., the crystal-lattice positions that hyperfine solute atoms will occupy in a compound, to learn if hyperfine tracers will be located in the lattice sites needed for an experiment, saving time and resources needed to perform experiments to learn the same information. Common applications of perturbed angular correlation spectroscopy (PAC) include detection of point defects and measuring atomic jump rates [1], and empirical simulations are particularly useful for calculating defect association enthalpies to predict which defects are likely to be attracted to hyperfine tracers and atomic migration barriers to predict which hyperfine tracers to select for measuring atomic jump rates in studies of diffusion.

In the wide variety of materials systems that one can contemplate investigating using PAC, or a closely related hyperfine method, intermetallic compounds provide a vast selection of systems with a range of interesting research topics. Over 600 binary intermetallic compounds form in the $B2$-, $L1_2$-, or $C15$-crystal structures alone [2]. Intermetallic compounds, which are also known as ordered alloys, can exhibit interesting modes of disorder; for example, several transition-metal $B2$ compounds are known to have a mixed vacancy-antisite disorder known as triple-defect disorder [3, 4], rather than the Schottky and antisite modes of disorder commonly found in nonmetallic compounds, yet the defect properties of most intermetallic compounds have not been investigated. Interesting defect association effects have been predicted. For example, transition-metal vacancies were observed to order at first-neighbor distances in NiAl [5] whereas they were predicted to order at second-neighbor distances in FeAl [6]. This effect was investigated using PAC [7, 8], but defect association in intermetallic compounds has not been studied widely beyond that. Finally, determination of diffusion mechanisms in intermetallic compounds has proved challenging, and hyperfine methods have the potential to provide important insight on this problem, provided that suitable hyperfine tracer-compound combinations can be identified [9].

It is, therefore, desirable to identify prospective intermetallic systems to investigate using hyperfine methods through computer simulation. A number of empirical-potential models have been developed to study metals and intermetallic compounds (for example, see Ref. [10], and references therein). Many are based on the embedded atom method (EAM), for which the total energy of a material is given by

$$E_{\text{total}} = \sum_i F_i\left(\overline{\rho}_i\right) + \frac{1}{2}\sum_{j\neq i}\phi_{ij}\left(r_{ij}\right) \qquad (1)$$

where i and j are summation indexes over atoms in the simulation space, F_i is the embedding function for atom i, $\overline{\rho}_i$ is the background electron density at the site atom i occupies, and $\phi_{ij}(r_{ij})$ is the short range pair interaction between atoms i and j when separated by distance r_{ij} [11, 12]. The functional forms of F_i, $\overline{\rho}_i$, and ϕ_{ij} vary among different implementations of the EAM. The present work uses an extension of the modified embedded atom method (MEAM) [13] known as the second-nearest neighbor (2NN) MEAM [14–16]. Some parameter sets based on MEAM are compatible with 2NN MEAM provided that they use the same functional form for the background density function and a correction to one of the electron density parameters is applied [17]. Potential parameters for 2NN MEAM, or compatible versions of MEAM, have been determined for some 39 different elements [18-39] (see Fig. 1), making 2NN MEAM an attractive candidate for exploring a large number of different intermetallic compounds and hyperfine-tracer elements.

Notably, a set of 2NN MEAM potential model parameters for cadmium, an important element for PAC, is not reported in the literature. The purpose of this work is to develop an interatomic potential for cadmium that could, at the very least, be used in simulations of atomic-scale defect properties of intermetallic compounds. This paper describes the methodology followed to derive a set of parameters, reports how well simulations based on this parameter set are able to reproduce known physical properties of cadmium, and discusses prospects for application of the potential for studying problems of interest to hyperfine researchers in the context of possible PAC experiments.

2 Methods

The functional forms of the terms that appear in Eq. 1 are readily available in the literature [9, 14–16]. There are 4 empirical parameters needed to calculate the short-range pair interaction: E_c, r_{1e}, α, and d; 10 empirical parameters needed to calculate the background electron density: $\beta^{(0)}$, $\beta^{(1)}$, $\beta^{(2)}$, $\beta^{(3)}$, $t^{(1)}$, $t^{(2)}$, $t^{(3)}$, $C_{\min}$, $C_{\max}$, and r_c; and 1 parameter needed for the embedding function: A; using the notation in Ref. [9]. Note that r_{1e} represents equilibrium atomic separation in the reference structure, which was taken as hexagonal close-packed (hcp) for cadmium in this work, since it is known from experiment that cadmium has the hcp structure.

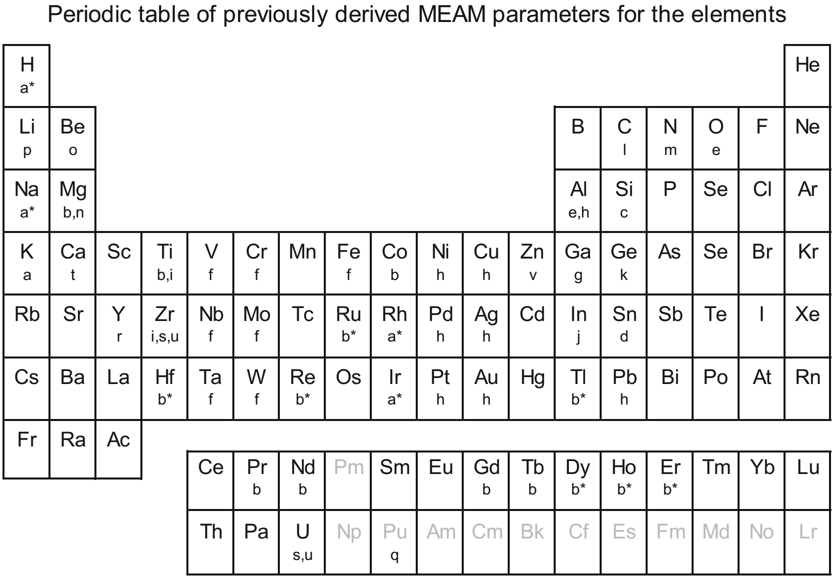

Periodic table of previously derived MEAM parameters for the elements

H a*																	He
Li p	Be o											B	C l	N m	O e	F	Ne
Na a*	Mg b,n											Al e,h	Si c	P	Se	Cl	Ar
K a	Ca t	Sc	Ti b,i	V f	Cr f	Mn	Fe f	Co b	Ni h	Cu h	Zn v	Ga g	Ge k	As	Se	Br	Kr
Rb	Sr	Y r	Zr i,s,u	Nb f	Mo f	Tc	Ru b*	Rh a*	Pd h	Ag h	Cd	In j	Sn d	Sb	Te	I	Xe
Cs	Ba	La	Hf b*	Ta f	W f	Re b*	Os	Ir a*	Pt h	Au h	Hg	Tl b*	Pb h	Bi	Po	At	Rn
Fr	Ra	Ac															
				Ce	Pr b	Nd b	Pm	Sm	Eu	Gd b	Tb b	Dy b*	Ho b*	Er b*	Tm	Yb	Lu
				Th	Pa	U s,u	Np	Pu q	Am	Cm	Bk	Cf	Es	Fm	Md	No	Lr

a: ref. [18]
b: ref. [19]
c: ref. [20]
d: ref. [21]
e: ref. [22]
f: ref. [23]
g: ref. [24]
h: ref. [25]
i: ref. [26]
j: ref. [27]
k: ref. [28]
l: ref. [29]
m: ref. [30]
n: ref. [31]
o: ref. [32]
p: ref. [33]
q: ref. [34]
r: ref. [35]
s: ref. [36]
t: ref. [37]
u: ref. [38]
v: ref [39]

*Potential parameters do not give the correct lowest-energy structure in simulations at finite temperature [16,39].

Fig. 1 Periodic table of previously derived empirical parameters compatible with the second nearest neighbor modified embedded atom method (2NN MEAM)

Determination of an optimal set of empirical parameters involved adjusting test-values until the potential model reproduced about 17 materials properties as closely as possible. In this work, all parameters were adjusted except for C_{max} and r_c, which were chosen to be 1.44 and 5.0 Å, respectively.

The initial set of parameters was chosen in part based on known properties of Cd metal. The theoretical cohesive energy and experimentally determined nearest neighbor distance were used as the starting values for E_c and r_{1e}. The experimentally determined bulk modulus B and atomic volume Ω were used to determine α. Values of 1.00 and 0.00 were chosen for A and d, respectively. Initially, $C_{min} = 1.00$ was used, which corresponds to no second neighbor screening. Remaining parameters were chosen based on values derived for other hcp-structured elements determined in earlier work [19].

Through a combination of trial-and-error and steepest-descent minimization, large ranges of possible values for parameters could be eliminated from consideration by comparison with structural and closely-related physical quantities such as lattice parameters, including c/a ratio and atomic volume, relative cohesive energies of the body-centered cubic (bcc), face-centered cubic (fcc), and hcp structures, and elastic constants of the hcp structure, all of which can be calculated quickly. Parameters were then refined by reproducing the vacancy formation enthalpy H_{vf}, surface enthalpies, H_{100} and H_{001}, and pressure dependence of bulk modulus, dB/dP. Final refinements were made, as needed, to reproduce as best as possible physical quantities that are more computationally expensive such as thermal expansion parameters and specific heat. In addition, molecular dynamics calculations of melting properties (temperature, volume change, and energy change) were performed as a final test of the broader applicability of the model.

The set of parameters found using the above procedure is given in Table 1. Values of Cd material properties calculated using this set of parameters are examined in the next section. All energy minimization calculations using the MEAM in this work were carried out using version 5.0 of the General Utility Lattice Program (GULP) [40, 41]. Molecular dynamics calculations were carried out using the LAMMPS software [42].

3 Calculation results

Calculations of cohesive enthalpy, structural properties, and elastic properties of hcp-, bcc-, and fcc-structured Cd were carried out at 0 K with unit cell parameters allowed to relax under constant pressure (taken to be 0 GPa). Values calculated for hcp-Cd and structural enthalpy differences between the polymorphs are given in Table 2.

Table 1 Values of the 2NN MEAM potential parameters for cadmium derived in this work

Parameter	Value	Parameter	Value
E_c	1.16 eV	$\beta^{(0)}$	1.73
r_{1e}	3.105 Å	$\beta^{(1)}$	–0.85
α	7.68	$\beta^{(2)}$	8.45
d	0.10	$\beta^{(3)}$	8.50
r_c	5.0 Å	$t^{(1)}$	16.2
A	1.02	$t^{(2)}$	–7.05
C_{min}	0.93	$t^{(3)}$	–1.80
C_{max}	1.44		

Table 2 Calculated bulk properties of cadmium metal

property	2NN MEAM	Experiment / Theory	Comment
E_c (eV)	1.16	1.16	Ref. [61]
a (Å)	2.900	2.979	Ref. [62]
c (Å)	5.927	5.617	Ref. [62]
c/a ratio	2.0437	1.8855	Calculated from lattice constants
Ω (Å^3)	21.587	21.585	Calculated from lattice constants
C_{11} (GPa)	128.4	114.5	Ref. [63]
C_{12} (GPa)	68.2	39.5	Ref. [63]
C_{13} (GPa)	19.2	39.9	Ref. [63]
C_{33} (GPa)	59.0	50.85	Ref. [63]
C_{44} (GPa)	39.0	19.85	Ref. [63]
B (GPa)	58.78	57.61	Calculated from elastic constants
(dB/dP)	7.12	7.19	From Rose's universal equation of state [43]
H(bcc)-H(hcp) (eV)	0.1562	0.0564	DFT (this work)
H(fcc)-H(hcp) (eV)	0.0176	0.0068	DFT (this work)

As can be seen, the present model overestimates the c/a ratio. The 2NN MEAM model is known to have difficulty reproducing c/a ratio in HCP compounds that have c/a ratios larger than the ideal value of 1.633 while simultaneously predicting that hcp is the lowest energy structure [19]. In a recent derivation of MEAM parameters for Zn, which, like Cd, has a large c/a ratio, the authors chose to parameterize their model based on the hcp structure with ideal c/a ratio, fitting to properties of that ideal structure as determined by density functional theory (DFT) [39]. It was found in the present work that it is also possible to get hcp as the lowest energy structure by overestimating the c/a ratio. This was the approach used here, because the percent difference between the overestimated c/a ratio and the experimental value of c/a is smaller than the percent difference of the ideal c/a ratio. While the c/a ratio calculated with the potential model is too large, the calculated atomic volume agrees well with the experimental value.

It was not possible to find a set of parameters that exactly reproduced elastic constants. This is, perhaps, to be expected given that the calculated c/a ratio is too large. It was possible to mostly reproduce the ordering $C_{11} > C_{33} > C_{12} \cong C_{13} > C_{44}$ found experimentally, except in the calculations $C_{12} > C_{13}$ and $C_{12} > C_{33}$. The average of C_{12} and C_{13}, however, falls into the relative ordering, and this average does not deviate substantially from the experimental values of C_{12} and C_{13}. Deviations between calculated and experimental values are of the same order as those in the study on Zn [39], and the bulk modulus reproduces the experimental value well. Also, the calculated value (dB/dP) is in good agreement with the value predicted using Rose's universal equation of state [43].

Conventionally, relative cohesive enthalpies of body-centered cubic (bcc), face-centered cubic (fcc), and hcp structures are used as tests of 2NN MEAM potential models. Therefore, in this work enthalpies of hcp-cadmium and of hypothetical bcc- and fcc-cadmium were calculated using the projector augmented-wave method [44, 45] implemented in the VASP code [46, 47]. Exchange-correlation effects were treated by the generalized gradient approximation of Perdew et al. [48]. All calculations were performed in high precision with the plane-wave cutoff energy set to 1.5 times the default PAW cutoff energy. Integration was performed using a Γ-centered grid of size 20 × 20 × 15 for the hcp structure and using the Monkhorst-Pack scheme [49] of size 22 × 22 × 22 for the fcc and bcc structures. Optimal lattice parameters were found by fitting enthalpy as a function of strain to the Birch-Murnaghan equation of state [50].

Differences in enthalpies obtained from the DFT calculations are given in Table 2 for comparison with values using the 2NN MEAM parameters. It was necessary to select a set of parameters that overestimate H(fcc) - H(hcp) in the MEAM calculations in order to stabilize the hcp structure with c/a ratio larger than the ideal value while simultaneously reproducing other physical properties of Cd. This, in turn, leads to a significant overestimation of H(bcc) - H(hcp). It is interesting that the degree of overestimation in H(bcc) - H(hcp) is comparable to the overestimation in the Zn study [39], even though it used a different approach to the c/a-related stability problem.

Calculation of vacancy formation enthalpy and entropy was done using 3 × 3 × 2-, 4 × 5 × 2-, 6 × 7 × 3-, 8 × 9 × 4-, and 10 × 12 × 5-dimension supercells, constructed using the calculated lattice parameters given in Table 2. Computations were done at constant volume with full relaxation of atomic coordinates to minimize enthalpy. Vibrational entropy was calculated using phonon frequencies at the Γ-point in the full harmonic approximation. Because experimental results are obtained under conditions of constant pressure, extra steps are necessary to determine these values based on constant-volume results. This can be done conveniently following the work of Mishin, Sørensen, and Voter [51].

The defect quantities-of-interest vary with supercell size, and their variations are proportional to $1/N$ where N is the number of atoms in the supercell. Calculated size dependences of vacancy formation enthalpy at constant volume, $(H_{\mathrm{vf}})_V$, and vacancy formation entropy at constant volume, $(S_{\mathrm{vf}})_V$ are shown in Figs. 2 and 3. Linear fits allow extrapolation to infinite supercell ($1/N = 0$). In this limit, the vacancy formation enthalpy at constant pressure, $(H_{\mathrm{vf}})_p$, is equal to $(H_{\mathrm{vf}})_V$. Entropy, however, is more complicated. The formation entropy at constant pressure, $(S_{\mathrm{vf}})_p$ can be calculated using

$$(S_{\mathrm{vf}})_p = (S_{\mathrm{vf}})_V + \beta B V_{\mathrm{vf}}, \tag{2}$$

where $(S_{\mathrm{vf}})_V$ is the formation entropy at constant volume, β is the thermal expansion factor at zero pressure, B is the bulk modulus, and V_{vf} is the vacancy-defect formation volume. Thus, in order to find $(S_{\mathrm{vf}})_p$, the thermal expansion factor and defect volume must also be calculated.

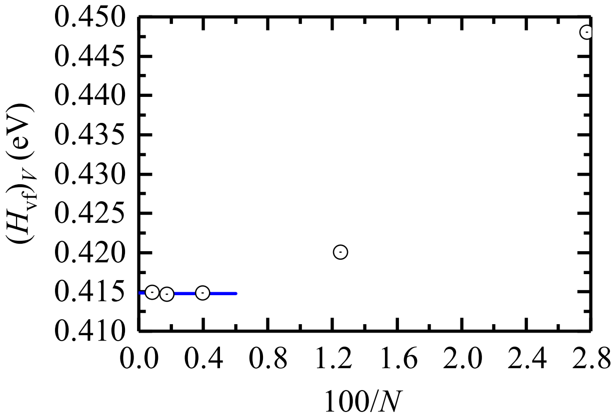

Fig. 2 Vacancy formation enthalpy dependence on supercell size, shown as a function of 100/N where N is the number of atoms in the supercell. The line indicates the result of a least-squares fit of the enthalpies calculated using the largest three supercells

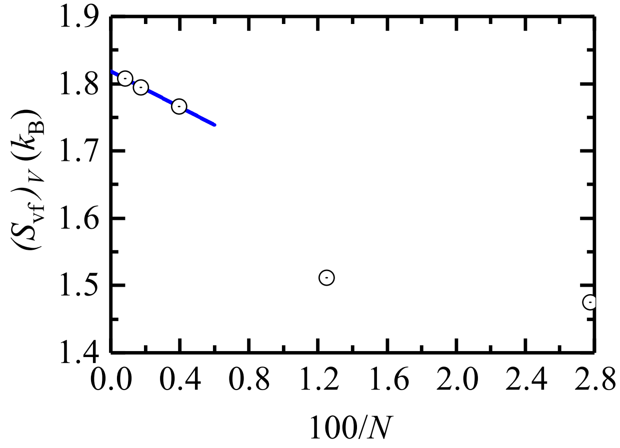

Fig. 3 Vacancy formation entropy dependence on supercell size, shown as a function of 100/N. The line indicates the result of a least-squares fit of the entropies calculated using the largest three supercells

The thermal expansion factor is given by

$$\beta = \frac{1}{B}\left(\frac{\partial S}{\partial V}\right)_T, \tag{3}$$

in terms of the volume derivative of entropy at constant temperature, which in the full harmonic approximation, is given by

$$\left(\frac{\partial S}{\partial V}\right)_T = -k_\mathrm{B}\sum_i \frac{1}{\nu_i}\left(\frac{d\nu_i}{dV}\right)_T, \tag{4}$$

where k_B is Boltzmann's constant and ν_i are the phonon frequencies. The $(d\nu_i/dV)_T$ factors are calculated conveniently by linear fits of the volume dependence of calculated phonon frequencies near the volume of the perfect lattice's supercell. Finally, the above equations are applied to calculate the thermal expansion factor for different sized supercells (Fig. 4) to determine its value at $1/N = 0$: $\beta = 6.0901(8) \times 10^{-5}\ \mathrm{K}^{-1}$.

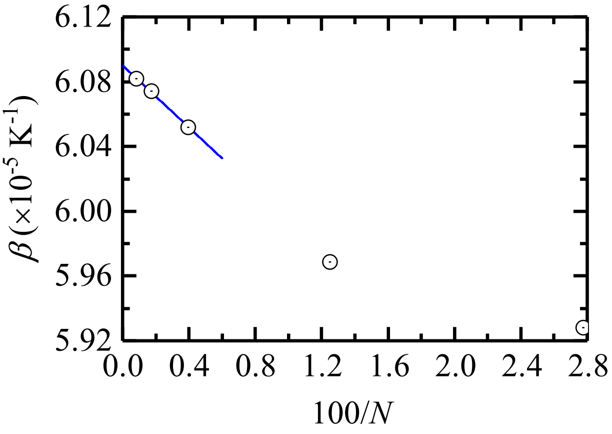

Fig. 4 Thermal expansion factor dependence on supercell size, shown as a function of 100/N. The line indicates the result of a least-squares fit to results from the largest three supercells

The relaxation volume of the vacancy is given by

$$V_{\mathrm{vf}} = -V_0 P / B, \tag{5}$$

where V_0 is the volume of the supercell, P is the sum of hydrostatic stresses on all atoms after relaxing atomic positions at constant volume, and B is still the isothermal bulk modulus [51]. As with the other defect quantities, V_{vf} is calculated at varying supercell sizes (Fig. 5), and the vacancy relaxation volume taken in the limit $N \rightarrow \infty$, which gives $V_{\mathrm{vf}} = -5(1)$ Å^3.

Calculated defect enthalpy and entropy at constant pressure are given in Table 3. As can be seen, there is excellent agreement between the calculated and the recommended experimental value for the formation enthalpy, and the calculated formation entropy is close to the recommended experimental value. In this case, the large uncertainty in entropy arises from the large uncertainty in vacancy relaxation volume.

Calculation of surface enthalpy on the 001 surface, H_{001} (or on a 100 surface, H_{100}) was performed by constructing a supercell consisting of 4 filled unit cells then 16 empty unit cells in the c (or a) direction. All atoms were allowed to fully relax at constant pressure. Results are given in Table 3, and, as can be seen, there is good agreement with experiment.

Free energy minimization was used to calculate thermal properties of Cd metal. Results are given in Table 4 for specific heat and thermal expansion coefficients. The calculations were performed on 3 × 3 × 2 supercells by varying lattice parameters until a minimum in Gibbs free energy at a given temperature was found. For each trial set of lattice parameters, atomic positions were allowed to fully relax to minimize enthalpy at constant volume. As in the defect calculations, vibrational entropy was calculated using phonon frequencies at the Γ-point in the full harmonic approximation. Specific heat, calculated using this procedure, is at constant volume. Specific heat at constant pressure is found using

$$C_p = C_V + VTB\beta^2, \tag{6}$$

where V is the volume of the supercell at minimum energy. As can be seen in Table 4, the calculated specific heat is in good agreement with experiment. Thermal expansion coefficients calculated using free energy minimization do not agree as well. A set of parameters that resulted in $\Delta c / c_0 / \Delta T$ significantly larger than $\Delta a / a_0 / \Delta T$, as observed experimentally, could not

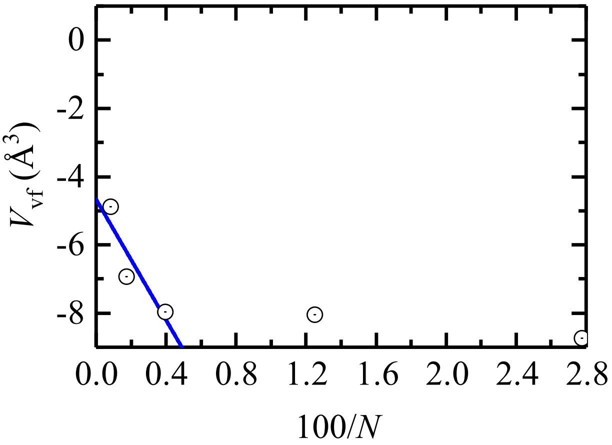

Fig. 5 Dependence of calculated vacancy relaxation volume on supercell size, shown as a function of 100/N. The line indicates the result of a least-squares fit to results from the largest three supercells

Table 3 Calculated defect and surface energies of cadmium metal

property	2NN MEAM	Experiment	Comment
$(H_{\mathrm{fv}})_p$ (eV)	0.41	0.39–0.52, 0.41 recommended	Ref. [64]
$(S_{\mathrm{fv}})_p$ (k_{B})	0.61	0.3–0.5, 0.4 recommended	Ref. [64]
H_{001} (eV/Å^2)	0.0515	0.04756	For polycrystalline from Ref. [65]
		0.04619	For polycrystalline from Ref. [66]
H_{100} (eV/Å^2)	0.0488	–	

be found. For parameter sets that reproduced other physical quantities well, there appeared to be an upper limit of roughly $\Delta c/c_0/\Delta T = 16 \times 10^{-6}$ K^{-1} when $\Delta a/a_0/\Delta T$ is near 17×10^{-6} K^{-1}. Such a choice in parameters leads to significant underestimation of $\Delta V/V_0/\Delta T$. The current set of parameters was chosen to deliberately overestimate $\Delta a/a_0/\Delta T$ in order to minimize underestimation of $\Delta V/V_0/\Delta T$ as much as possible while satisfactorily reproducing other physical quantities. Thermal expansion coefficients obtained from molecular dynamics calculations, described below, are also shown in Table 4, and the volume coefficient is in better agreement with experiment. The discrepancy between free-energy and molecular-dynamics results likely are due to the use of a relatively small supercell in the free-energy calculations.

Molecular dynamics simulations were performed primarily to determine melting temperature and changes in enthalpy and volume upon melting. The melting temperature was found using a solid-liquid interface method [52, 53], the first step of which requires direct-heating and direct-cooling simulations, which also allows calculation of enthalpy and volume changes along with thermal expansion coefficients.

Direct-heating on an 8 × 14 × 6 supercell with 2016 atoms at a rate of 0.5 K/ps was performed under constant pressure using a time step of 1 fs and NPT ensemble with Nose-Hoover thermostat and barostat parameter values of 0.1 ps and 2.0 ps, respectively. The system was allowed to equilibrate at 200 K for 100 ps before heating. The volume dependence on simulation temperature averaged over 0.5 ps intervals is shown in Fig. 6. As can be seen by the rapid increase in volume between 770 and 790 K, the simulation cell melts around 780 K. This cannot be used as the basis of determining the melting temperature, however, because it is known that superheating of the simulation system occurs when direct-heating methods are used, leading to overestimation of melting temperature [53, 54].

Starting with the atomic positions and velocities of liquid Cd at 1200 K from the direct-heating simulation output, a direct-cooling simulation on the liquid was performed. It used the NPT ensemble with thermostat and barostat parameter values of 0.1 ps and 1.0 ps. The system

Table 4 Thermal properties of cadmium metal. Thermal expansion parameters were calculated using two different methods: free energy minimization (EM) and molecular dynamics (MD)

property	2NN MEAM	Experiment	Comment
C_{v} (300 K) (eV/K)	0.0002446		
C_{p} (300 K) (eV/K)	0.0002534	0.0002695	Refs. [63, 67, 68]
$\Delta a/a_0/\Delta T$ (300–400 K) ($\times 10^{-6}$ K^{-1})	21.9 (EM) 23.9 (MD)	17.4	Ref. [69]
$\Delta c/c_0/\Delta T$ (300–400 K) ($\times 10^{-6}$ K^{-1})	18.3 (EM) 23.9 (MD)	43.6	Ref. [69]
$\Delta V/V_0/\Delta T$ (300–400 K) ($\times 10^{-6}$ K^{-1})	62.2 (EM) 71.7 (MD)	78.4	Calculated from linear terms

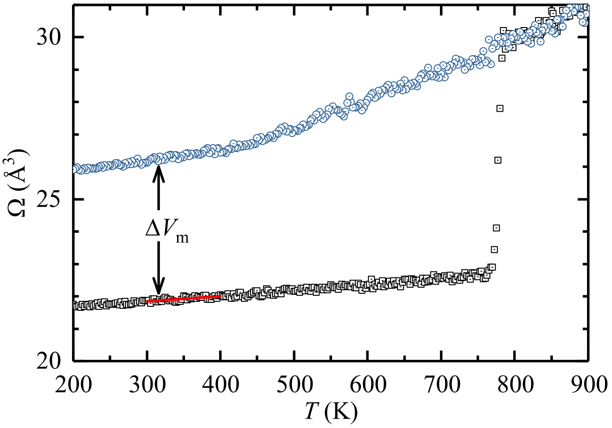

Fig. 6 Atomic volume determined from molecular dynamics as a function of simulation target temperature. Square symbols are for direct heating of the solid and circles are for direct cooling in the liquid phase. The line indicates the best fit of volume in the solid phase between 300 and 400 K

was cooled at a rate of 0.5 K/ps. The volume dependence on simulation temperature averaged over 0.5 ps intervals is are shown in Figs. 6. As can be seen, there was not a sudden drop in volume indicating crystallization during the simulation, which is not unexpected given that crystal-nucleation events are rare occurrences in MD simulations [54].

The simulation supercell for the solid-liquid interface at a given temperature was constructed by stacking in the *c*-direction a snapshot of the solid taken during the direct-heating simulation and a snapshot of the liquid taken from the direct-cooling simulation. The liquid's cell was distorted to match the lateral dimensions of the solid's cell with the liquid cell's *c* parameter allowed to expand to preserve the liquid cell's volume. For a target temperature far from the system's equilibrium melting temperature, the solid will melt during a simulation at constant pressure and temperature. When near the equilibrium transition temperature, simulations at constant volume and energy yield equilibrium pressure and temperature, which, because the liquid and solid phases coexist, gives the melting temperature at the pressure of the simulation.

Simulations were performed at selected temperatures below 770 K to check if the solid melts within a 5-ns simulation duration using a time step of 1 fs and NPT ensemble with thermostat and barostat parameter values of 0.1 ps and 2.0 ps. Above 350 K, the simulation melts or largely melts within 5 ns, indicating that the true melting temperature, according to the 2NN MEAM model, is below 350 K.

Additional interface simulations were performed between 275 and 350 K to obtain an estimate of the melting temperature. At each temperature, a solid-liquid supercell was constructed as described above, and a three-step molecular dynamics calculation performed: (1) a 500-ps simulation using the NPT ensemble with thermostat and barostat parameter values of 0.1 ps and 2.0 ps to remove any high-energy boundary states created in the construction of the supercell, (2) a 200-ps simulation using the NVT ensemble with 0.1 ps thermostat parameter, and (3) a 1 ns simulation using the NVE ensemble, with temperature and pressure calculated by averaging over the final 600 ps. The above steps were performed 40 times for each temperature, and results averaged to produce the pressure-temperature relation shown in Fig. 7. A linear-least squares fit to this data gives the approximate melting temperature: $T_m = 315(6)$ K.

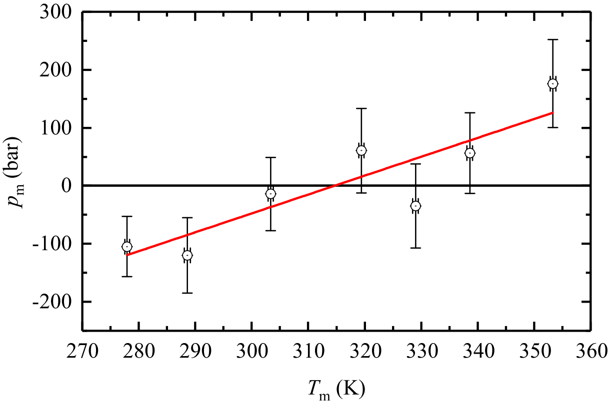

Fig. 7 Calculated melting temperature and pressure using the solid-liquid interface method. The best-fit line is indicated

Using this value of T_m, the change in volume at the melting temperature can be found from volumes calculated in the direct heating and cooling simulations. The change in volume ΔV_m is labeled in Fig. 6. The fractional change in volume, $\Delta V_m/V_{solid}$, is found to be about 21%. In principle, the change in enthalpy at the melting temperature can found from the enthalpies obtained in the direct heating and cooling simulations. The temperature-dependence of these enthalpies are shown in Fig. 8. Also shown in Fig. 8 are linear fits of the temperature dependence determined between 200 and 500 K for the solid phase and between 700 and 1200 K for the liquid. It is not understood why the calculated enthalpy of the liquid deviates from the best-fit line below 700 K. The lines of best fit were used to determine the change in enthalpy ΔH_m to be about 0.01 eV, which is much lower than the experimental value. Results of predicted melting temperature and related quantities are summarized in Table 5.

Finally, thermal expansion coefficients can be calculated using results from the direct heating simulation. A linear fit of volume versus temperature between 300 and 400 K, shown in Fig. 6 allows calculation of $\Delta V/V_0/\Delta T$. Similarly, linear fits of the temperature dependences

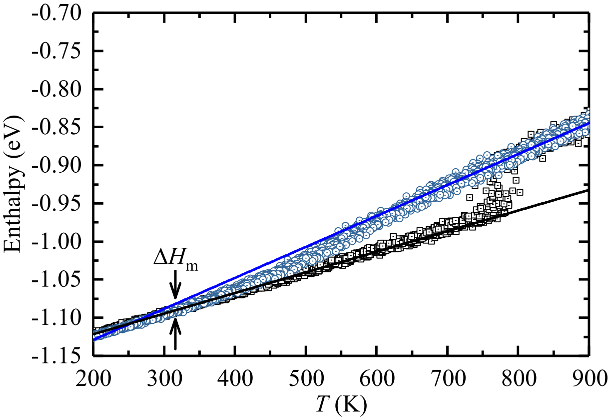

Fig. 8 Enthalpy per atom determined by molecular dynamics as a function of simulation target temperature. Square symbols are for direct heating of the solid and circles are for direct cooling in the liquid phase. Lines indicate best fits to determine the change in enthalpy at the melting temperature. Enthalpy of the solid was fitted over the range 200–500 K, and the liquid was fitted over the range 700–1200 K

Table 5 Properties of cadmium metal at its melting temperature

property	2NN MEAM	Experiment	Comment
T_m (K)	315(6)	594	Refs. [63, 68]
ΔH_m (eV)	0.01	0.08911	Ref. [67]
		0.0643	Ref. [63]
		0.0664	Ref. [68]
$\Delta V_m/V_{solid}$	21%	4.0%	Ref. [68]

of a and c lattice parameters, shown in Fig. 9 allows determination of $\Delta a/a_0/\Delta T$ and $\Delta c/c_0/\Delta T$. Results are given in Table 4 and values are closer to experiment than those obtained using the free energy method, again, likely because of the small supercell used in the free energy calculations.

4 Discussion

The overall agreement between values calculated using the potential parameter set in Table 1 and known experimental and theoretical values in Tables 2, 3, and 4 is comparable to what has been reported in other derivations of 2NN MEAM potentials [18–38]. The agreement of melting temperature and related properties in Table 5, however, is generally worse than what is reported in the literature [14, 19, 21, 24, 25, 27, 28, 31—33, 37, 39]. The absolute error in melting temperature varies greatly among MEAM simulations of other work, and the error of −279 K in this work is not completely out of line with other work. However, the deviations in ΔH_m and ΔV_m are unsatisfactorily large compared with errors reported in other simulations. This indicates that results should be treated with caution if this potential is used for phase stability calculations.

It is known that a potential-parameter set for the modified embedded atom method that correctly predicts the stable structure at 0 K may not predict the correct stable structure at finite temperature [14, 16, 39]. That is, it is possible to derive a set of parameters that correctly

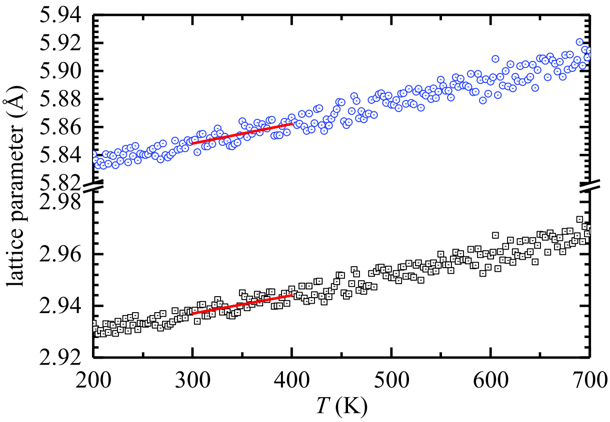

Fig. 9 Lattice parameters determined from of molecular dynamics as a function of simulation target temperature. Square symbols are for direct heating of the solid and circles are for direct cooling in the liquid phase. Lines indicate best fit lines in the 300–400 K temperature range

predicts the most stable structure at 0 K, but then free energy minimization or molecular dynamics calculations using that potential set will give a different stable structure above 0 K. This was tested for the current potential set by free energy minimization of the most common metal structures, hcp, bcc, and fcc; of orthogonally distorted bcc and fcc; and of the B19 structure, which was found to be the most stable structure at high temperature using earlier potential models for hcp-structured metals [39]. Calculation results, reported in energy per atom, at 50 K increments are given in Fig. 10 using 2 × 2 × 2 supercells for all structures except hcp, for which a 3 × 3 × 2 supercell was used. As can be seen, hcp has the lowest energy, and, therefore, is the most stable structure at finite temperature up to 400 K. At 450 K and above, the B19 structure is the most stable.

This changeover in stable structure indicates that molecular dynamics simulations and free energy minimization carried out at finite temperature are only reliable for solid hcp-Cd up to about 400 K, though results above 316 K are not in thermodynamic equilibrium. Moreover, it indicates materials properties calculated at room temperature and calculations of defect-enthalpy and vibrational-entropy using the energy minimization method described in this work should be reliable.

Because the potential model set in Table 1 is satisfactory for predicting structural, elastic, and defect properties of Cd metal, it is expected to be reliable for predicting behavior of Cd solutes in other intermetallic compounds. Tests of the potential-model parameters in alloys are underway using a refinement of the scheme for parameterizing binary pairs described in Ref. [9]. The first step is to check accuracy of predicted materials properties of ordered-alloys for the limited set of compounds formed between Cd and other elements for which 2NN MEAM potentials have been derived (Fig. 1). Further potential-model validation will be possible through calculation of cadmium site occupation behavior in other binary intermetallic compounds and testing of those predictions by performing perturbed angular correlation experiments using ^{111m}Cd and by comparing to predictions made using DFT. A good first candidate for this is to examine Cd behavior in Pd_3Ga_7 for comparison with experimental results [55] and site occupation and defect association enthalpies calculated using DFT. In addition to providing a means of testing the efficacy of the potential, follow-up calculations of Cd migration

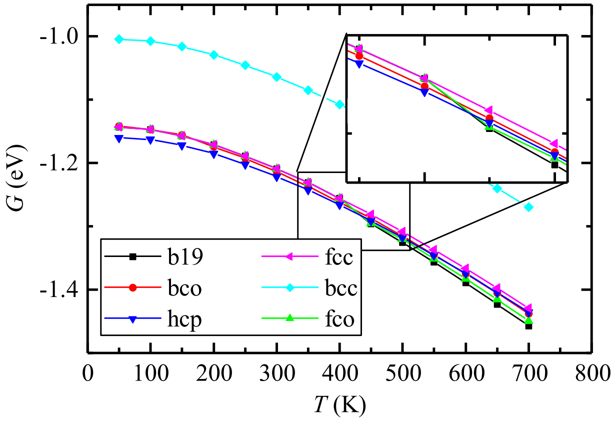

Fig. 10 Calculated Gibbs free energy per atom for a selection of Cd polymorphs. The hcp structure has the lowest energy, and is therefore the most stable structure according to the calculations up to just over 400 K. Above that, the B19 structure is most stable

barriers along different diffusion pathways in Pd_3Ga_7 may provide an explanation why there was a factor 4 difference in Cd jump rates on the two Ga sublattices observed using PAC [55].

An attractive application of the new Cd potential is to investigate the nature of the reported change in diffusion behavior of Cd in the rare earth tri-indide series [56]. In that work, Cd jump rates were determined by measuring nuclear quadrupole relaxation using PAC. Larger relaxation, which corresponds to faster Cd jumps, was observed in the heavy rare-earth compounds for compositions more deficient in indium, as would be expected for diffusion mediated by vacancies on the In sublattice. In contrast, greater relaxation was observed for light rare-earths (La, Ce, and Pr) for compositions with excess In, suggesting Cd diffusion is mediated in those compounds by a different mechanism [57]. An alternative interpretation of the larger-than-expected relaxation observed in the In-rich compounds is that it is due to a shift of Cd site occupation away from the In sublattice within nanoseconds of the ^{111}In-to-^{111}Cd decay process [58]. While preliminary calculations using DFT provide some insight into these possible interpretations [59, 60], a full analysis requires calculation of phonon frequencies and migration barriers along different possible diffusion pathways using, ideally, large supercells to eliminate systematic errors created by interactions between defects and their images in adjacent supercells. Such calculations are more computationally tractable using a model with empirical potentials, such as the 2NN MEAM, than with DFT, and the Cd potential derived in this work will play a key role in such simulations.

5 Summary

An interatomic potential for cadmium based on the 2NN MEAM has been derived. The empirical parameters of the potential were determined through optimization of the parameter set's ability to reproduce known physical properties of pure cadmium. The potential parameter set satisfactorily reproduces physical properties of cadmium including cohesive energy, lattice parameters, elastic constants, structural enthalpy differences, surface enthalpy, vacancy formation energy, thermal expansion coefficients, and specific heat. While the potential does not describe melting temperature and changes in material properties upon melting well, it is expected to be reliable for predicting behavior of Cd solutes in intermetallic compounds. This makes it possible to employ the potential in future simulations to help interpret results of previous PAC measurements of Cd jump rates in Pd_3Ga_7 and in rare earth tri-indides and to guide selection of other intermetallic compounds likely to produce interesting experimental results when using PAC.

Acknowledgements This work is supported in part by NSF grant DMR 15-08189. The author would like to thank David Maess for his help investigating if melting properties could be reproduced better by using a set of 2NN MEAM potential parameters that underestimate *c*/*a* ratio of Cd.

References

1. Zacate, M.O., Jaeger, H.: Perturbed Angular Correlation Spectroscopy – a Tool for the Study of Defects and Diffusion at the Atomic Scale. Defect Diffus. Forum. **311**, 3–38 (2011)
2. Villars, P.: Pearson's Handbook Desk Edition: Crystallographic Data for Intermetallic Phases (ASM International: Materials Park, OH, 1997)

3. Haraguchi, T., Kogachi, M.: Point defect behavior in B2-type intermetallic compounds. Mater. Sci. Eng. A. **329–331**, 402–407 (2002)
4. Huang, M., Xie, F., Yan, X., Chang, Y.A.: Vacancy concentrations in the B2 intermetallic phase PdIn at 900°C. Intermetallics. **9**, 457–460 (2001)
5. Georgopoulos, P., Cohen, J.B.: The defect arrangement in (nonstoichiometric) β'-NiAl. Acta Metall. **29**, 1535–1551 (1981)
6. Fähnle, M., Meyer, B., Bester, G., Majer, J., Bornsen, N.: Atomic defects and electronic structure of B2 FeAl, CoAl and NiAl. Diffusion and Defect Data—Solid State Data, Pt. A: Defect and Diffusion Forum **194–199**, 279–286 (2001)
7. Zacate, M.O., Collins, G.S.: Vacancy-vacancy interactions in NiAl. Defect Diffus. Forum. **194–199**, 383–388 (2001)
8. Collins, G.S., Peng, L.S.-J., Zacate, M.O.: Point defects in FeAl studied by perturbed angular correlation. Defect Diffus. Forum. **213–215**, 107–231 (2003)
9. Zacate, M.O.: Indium-defect interactions in FCC and BCC metals studied using the modified embedded atom method. Hyperfine Interact. **237**, 131/1–13 (2016)
10. Ryu, S., Cai, W.: Comparison of Thermal Properties Predicted by Interatomic Potential Models. Model. Simul. Mater. Sci. Eng. **16**, 085005/1–12 (2008)
11. Daw, M.S., Baskes, M.I.: Embedded-atom method: Derivation and application to impurities, surfaces, and other defects in metals. Phys. Rev. B. **29**, 6443–6453 (1984)
12. Daw, M.S., Baskes, M.I.: Semiempirical, quantum mechanical calculation of hydrogen embrittlement in metals. Phys. Rev. Lett. **50**, 1285–1288 (1983)
13. Baskes, M.I.: Modified embedded-atom potentials for cubic materials and impurities. Phys. Rev. B. **46**, 2727–2742 (1992)
14. Lee, B.-J., Baskes, M.I.: Second nearest-neighbor modified embedded-atom-method potential. Phys. Rev. B. **62**, 8564–8567 (2000)
15. Lee, B.-J., Baskes, M.I., Kim, H., Cho, Y.K.: Second nearest-neighbor modified embedded atom method potentials for bcc transition metals. Phys. Rev. B. **64**, 184102, (2001)
16. Lee, B.-J., Shim, J.-H., Baskes, M.I.: Semiempirical atomic potentials for the fcc metals Cu, Ag, Au, Ni, Pd, Pt, Al and Pb based on first and second nearest-neighbor modified embedded atom method. Phys. Rev. B. **68**, 144112 (2003)
17. Baskes, M.I.: Atomistic potentials for the molybdenum-silicon system. Mater. Sci. Eng. A. **261**, 165–168 (1999)
18. Baskes, M.I.: Modified embedded-atom potentials for cubic materials and impurities. Phys. Rev. B. **46**, 2727–2742 (1992)
19. Baskes, M.I., Johnson, R.A.: Modified embedded atom potentials for HCP metals. Model. Simul. Mater. Sci. Eng. **2**, 147–163 (1994)
20. Lee, B.-J.: A modified embedded atom method interatomic potential for silicon. CALPHAD **31**, 95–104 (2007)
21. Ravelo, R., Baskes, M.: Equilibrium and Thermodynamic Properties of Grey, White, and Liquid Tin. Phys. Rev. Lett. **79**, 2482–2485 (1997)
22. Baskes, M.I.: Modified embedded atom method calculations of interfaces. Technical Report SAND-96-8484C; CONF-9603153-1 (Sandia National Laboratories: Livermore, USA, 1996, https://www.osti.gov/biblio/224267)
23. Lee, B.-J., Baskes, M.I., Kim, H., Cho, Y.K.: Second nearest-neighbor modified embedded atom method potentials for bcc transition metals. Phys. Rev. B. **64**, 184102 (2001)
24. Baskes, M.I., Chen, S.P., Cherne, F.J.: Atomistic model of gallium. Phys. Rev. B. **66**, 104107 (2002)
25. Lee, B.-J., Shim, J.-H., Baskes, M.I.: Semiempirical atomic potentials for the fcc metals Cu, Ag, Au, Ni, Pd, Pt, Al and Pb based on first and second nearest-neighbor modified embedded atom method. Phys. Rev. B. **68**, 144112 (2003)
26. Kim, Y.-M., Lee, B.-J., Baskes, M.I.: Modified embedded-atom method interatomic potentials for Ti and Zr. Phys. Rev. B. **74**, 014101 (2006)
27. Do, E.C., Shin, Y.-H., Lee, B.-J.: A modified embedded-atom method interatomic potential for indium. CALPHAD **32**, 82–88 (2008)
28. Kim, E.H., Shin, Y.-H., Lee, B.-J.: A modified embedded-atom method interatomic potential for Germanium. CALPHAD **32**, 34–42 (2008)
29. Lee, B.-J., Lee, J.W.: A modified embedded-atom method interatomic potential for carbon. CALPHAD **29**, 7–16 (2005)
30. Lee, B.-J., Lee, T.-H., Kim, S.-J.: A modified embedded-atom method interatomic potential for the Fe-N system: A comparative study with the Fe-C system. Acta Mater. **54**, 4597–4607 (2006)

31. Kim, Y.-M., Kim, N.J., Lee, B.-J.: Atomistic modeling of pure Mg and Mg-Al systems. CALPHAD **33**, 650–657 (2009)
32. Thompson, A.P., Lane, J.M.D., Desjarlais, M.P., Baskes, M.I.: Molecular dynamics simulation of dynamic response of beryllium. AIP Conf. Proc. **1195**, 833–836 (2009)
33. Kim, Y.-M., Jung, I.-H., Lee, B.-J.: Atomistic modeling of pure Li and Mg-Li system. Model. Simul. Mater. Sci. Eng. **20**, 035005/1–13 (2012)
34. Baskes, M.I.: Atomistic model of plutonium. Phys. Rev. B. **62**, 15532–15537 (2000)
35. Ko, W.-S., Lee, B.-J.: Modified embedded-atom method interatomic potentials for pure Y and the V-Pd-Y ternary system. Model. Simul. Mater. Sci. Eng. **21**, 085008/1–18 (2013)
36. Moore, A.P., Beeler, B., Baskes, M., Okuniewski, M., Deo, C.S.: Atomistic Ordering in Body Centered Cubic Uranium-Zirconium Alloy. Mater. Res. Soc. Symp. Proc. **1514**, 27–35 (2013)
37. Kim, K.-H., Jeon, J.B., Lee, B.-J.: Modified embedded-atom method interatomic potentials for mg-X (X=Y, Sn, ca) binary systems. CALPHAD. **48**, 27–34 (2015)
38. Moore, A.P., Beeler, B., Deo, C., Baskes, M.I., Okuniewski, M.A.: Atomistic modeling of high temperature uranium-zirconium alloy structure and thermodynamics. J. Nucl. Mater. **467**, 802–819 (2015)
39. Jang, H.-S., Kim, K.-M., Lee, B.-J.: Modified embedded-atom method interatomic potentials for pure Zn and Mg-Zn binary system. Calphad. **60**, 200–207 (2018)
40. Gale, J.D.: GULP - a computer program for the symmetry adapted simulation of solids. JCS Faraday Trans. **93**, 629 (1997)
41. Gale, J.D., Rohl, A.L.: The General Utility Lattice Program. Mol. Simul. **29**, 291–341 (2003)
42. Plimpton, S.: Fast Parallel Algorithms for Short-Range Molecular Dynamics. J. Comput. Phys. **117**, 1–19 (1995) http://lammps.sandia.gov
43. Rose, J.H., Smith, J.R., Guinea, F., Ferrante, J.: Universal features of the equation of state of metals. Phys. Rev. B. **29**, 2963–2969 (1984)
44. Blöchl, P.E.: Projector augmented-wave method. Phys. Rev. B. **50**, 17953 (1994)
45. Kresse, G., Joubert, J.: From ultrasoft pseudopotentials to the projector augmented wave method. Phys. Rev. B. **59**, 1758 (1999)
46. Kresse, G., Hafner, J.: Ab initio molecular dynamics for liquid metals. Phys. Rev. B. **47**, 558 (1993)
47. Kresse, G., Furthmüller, J.: Efficient iterative schemes for ab initio total-energy calculations using a plane-wave basis set. Phys. Rev. B. **54**, 11169 (1996)
48. Perdew, J.P., Chevary, J.A., Vosko, S.H., Jackson, K.A., Pederson, M.R., Singh, D.J., Fiolhais, C.: Atoms, molecules, solids, and surfaces: Applications of the generalized gradient approximation for exchange and correlation. Phys. Rev. B. **46**, 6671 (1992)
49. Monkhorst, H.J., Pack, J.D.: Special points for Brillouin-zone integrations. Phys. Rev. B. **13**, 5188 (1976)
50. Birch, F.: Finite elastic strain of cubic crystals. Phys. Rev. **71**, 809–824 (1947)
51. Mishin, Y., Sørensen, M.R., Voter, A.F.: Calculation of point-defect entropy in metals. Philos. Mag. A. **81**, 2591–2612 (2001)
52. Morris, J.R., Song, X.: The melting lines of model systems calculated from coexistence simulations. J. Chem. Phys. **116**, 9352–9358 (2002)
53. Zhang, Y., Maginn, E.J.: A comparison of methods for melting point calculation using molecular dynamics simulations. J. Chem. Phys. **136**, 144116/1–12 (2012)
54. Alavi, S., Thompson, D.L.: Simulations of melting of polyatomic solids and nanoparticles. Mol. Simul. **32**, 999–1015 (2006)
55. Nieuwenhuis, E.R., Zacate, M.O., Collins, G.S.: Simultaneous measurement of tracer jump frequencies on different sublattices in Ga_7Pd_3 using PAC. Defect Diffus. Forum. **264**, 27–32 (2007)
56. Collins, G.S., Jiang, X., Bevington, J.P., Selim, F., Zacate, M.O.: Change of diffusion mechanism with lattice parameter in the series of lanthanide indides having $L1_2$ structure. Phys. Rev. Lett. **102**, 155901 (2009)
57. Zacate, M.O., Favrot, A., Collins, G.S.: Atom Movement in In_3La Studied Via Nuclear Quadrupole Relaxation. Phys. Rev. Lett. **92**, 225901 (2004); Erratum, Phys. Rev. Lett. **93**, 49903 (2004)
58. Collins, G.S.: Diffusion and Equilibration of Site-Preferences Following Transmutation of Tracer Atoms. Diffusion Foundations. **19**, 61–79 (2019)
59. Bevington, J.P.: Lattice locations and diffusion in intermetallic compounds explored through PAC measurements and DFT calculations (PhD Dissertation, Washington State University, 2011)
60. Zacate, M.O., Bevington, J.P., Collins, G.S.: Simulation of Intrinsic Defects and Cd Site Occupation in $LaIn_3$ and $LuIn_3$ (submitted to Diffusion Foundations)
61. Kittel, C.: Introduction to Solid State Physics, 7th edn. John Wiley & Sons, Inc., New York (1996)
62. Lynch, R.W., Drickamer, H.G.: The effect of pressure on the resistance and lattice parameters of cadmium and zinc. J. Phys. Chem. Solids. **26**, 63–68 (1965)
63. Haynes, W.M., Lide, D.R.: CRC Handbook of Chemistry and Physics. CRC Press, Boca Raton (2010)

64. Siegel, R.W.: Vacancy Concentrations in Metals. J. Nucl. Mater. **69&70**, 117–146 (1978)
65. Tyson, R.W., Miller, W.A.: Surface free energy of solid materials: estimation from liquid surface tension measurements. Surf. Sci. **62**, 267–276 (1977)
66. de Boer, F.R., Boom, R., Mattens, W.C.M., Miedema, A.R., Niessen, A.K.: Cohesion in Metals. North-Holland, Amsterdam (1988)
67. Dinsdale, A.T.: SGTE Data for Pure Elements. CALPHAD. **15**, 317–425 (1991)
68. Gale, W.F., Totemeier, T.C.: Smithells Metals Reference Book, 8th edn. Elsevier, Amsterdam (2004)
69. Janot, C., George, B.: Equilibrium concentrations of vacancies in hexagonal metals. Phys. Rev. B. **12**, 2212–2219 (1975)